A New Hysteresis Simulation Method for Interpreting the Magnetic Properties of Non-Oriented Electrical Steels

Z.Zhang [a*], H. Hamzehbahmani [a], P. H. Gaskell [a]

[a] Department of Engineering, Durham University, Durham, DH1 3LE, UK

ARTICLEINFO

Article history:

Keywords:
Hysteresis simulation
Non-oriented electrical steels
Magnetic losses

ABSTRACT

The magnetic properties of non-oriented electrical steels are characterized using an analytical simulation method accounting for the microstructures in ferromagnetic materials. Complementary experimental data for thin sheet laminations, obtained using a standard single strip tester (SST), are employed with the hysteresis mechanism investigated in terms of the measurement system and Weiss Mean Field effects. It is shown that the magnetic hysteresis loops of NOESs of 3 % SiFe can be generated with remarkable accuracy for a broad range of magnetization frequencies and peak flux densities. The simulation method is also suitable for performing an energy loss analysis with calculated energy losses, when compared to corresponding measured data, showing a strikingly accurate match with, in most cases, an error of less than 1%.

1. Introduction

Electrical steels are the most suitable ferromagnetic material for the manufacture of the magnetic cores of various electromagnetic devices. They can be divided into two categories based on their microscopic grain structures: non-oriented electrical steel (NOES) and grain-oriented electrical steel (GOES). The magnetic properties of NOES are roughly the same in any magnetization direction in the plane of the material because of the arbitrarily oriented grain directions [1]. NOES laminates are widely used in industry, from large motors and generators that require good isotropic magnetic properties to EI laminates for small transformers. Due to the accelerating electrification of the world and increasing emphasis on electrical motor performance, NOESs will play a vital role in future energy systems, especially in relation to electric vehicles to achieve zero carbon emission. Therefore, the accurate analysis and numerical modelling of the magnetic behavior of NOESs is crucial for studying the magnetization processes and performance of ferromagnetic materials within the magnetization range of practical interest.

The magnetization processes of ferromagnetic materials can be accurately analyzed using the hysteresis phenomenon [2,3]. The physical origin of hysteresis has been of interest to scientists for over a century since the term hysteresis was coined around 1900 by Sir James Alfred Ewing [4]. The attribution of magnetic hysteresis to eddy currents was proposed because the counter field, which is opposite to the magnetic induction, is generated by the eddy currents when a steel laminate is magnetized [5]. The most widespread assumption of attribution of hysteresis is the pinning site effect, which impedes domain wall movement and causes the magnetization to be asynchronous to the magnetic field [6-8]. An assertion cited from [9] suggests that lattice defects and the eddy current effect result in the pinning effect, which dominates the irreversible domain wall displacement associated with hysteresis loops. The causation of magnetic hysteresis was also described in [10] using a friction force due to the pinning effect of Bloch walls. Positive feedback theory contributing to the origin of hysteresis is presented in [11]; this quantum mechanism of hysteresis was established based on the Weiss Mean Field (WMF) due to the coupling effect of atomic dipoles [12]. Because the pinning site effects or dry-friction force always exert negative feedback effects, the theories in [6-10] and [11] are contradictory. To date, which of the above theories is correct has yet to be definitively answered.

The Jiles-Atherton (J-A) model [13] was proposed based on the assumption of overcoming the impedance pinning of domain wall motion. It can be used to simulate the hysteresis loop independently for homogenous materials because the anhysteretic magnetization equation is derived for isotropic materials [14]. Two differential equations are used to represent irreversible and reversible differential susceptibilities, their combination resulting in the total differential susceptibility [14]. However, this model is not suitable for inhomogeneous anisotropic structures. Ramesh [15] and Szewczyk [16] extended the J-A model to include anisotropic magnetic materials by introducing anisotropic energy to the anhysteretic magnetization

[n] Corresponding author.
E-mail address:
zz1v22@soton.ac.uk (Z.Zhang)
zhi.zhang@durham.ac.uk (Z.Zhang).

equation. The extension makes it possible to trace the magnetic hysteresis of anisotropic materials.

Mathematical models utilizing operators, such as the Preisach [17] and vector Preisach models [18], or the Stop and Play models [19], are not linked to the physics of magnetic materials. The Preisach model represents magnetic hysteresis with reasonable accuracy for tracing hysteresis loops, which has led to it being widely used for the analysis of magnetization. [20] proposes a hybrid model of dynamic magnetic hysteresis, which combines the dynamic J-A and Preisach models based on backpropagation neural networks.

The authors recently presented a new hysteresis simulation method [21] developed according to the assumption that the hysteresis field is the coupling effect of magnetization at the reversal turning point, which is the WMF at the magnetic flux density tips, which are the transition points from magnetization to demagnetization. The WMF executes a counterforce (negative feedback) to the magnetic field when it manages to reverse the direction of magnetic flux density. The simulation method derived was based on the microscopic variations in the ferromagnetic materials subjected to an external magnetic field. The simulation method was used to simulate the hysteresis loops and evaluate the energy loss.

This paper presents a new analytical simulation method in the form of a single equation to describe the magnetic behaviour of NOESs. Its main advantage is that the parameters involved represent the microstructure of the magnetic materials, i.e., the domain patterns, which enable the simulation of the hysteresis loops with high accuracy. The method can be used to characterize the magnetization processes and enable an energy loss prediction of NOESs with remarkable accuracy.

2. Measurement system and hysteresis mechanism

A standard single strip tester (SST) was used to magnetize Epstein size laminations of NOES samples based on the BS EN 10280:2001 + A1:2007 [22, 23]. Epstein size laminations (30 mm × 305 mm) of NO 3% SiFe with a thickness of d=0.5 mm and resistivity ρ=0.3 μΩ-m were used in this work. Fig. 1 illustrates the computer-controlled measuring system used to monitor the measuring processes. The magnetization processes were controlled and monitored using reliable software. The computer system is linked to the SST through a data acquisition Card (DAC). The excitation current was supplied by a power amplifier to the primary winding, and a 1 Ω shunt resistor (Rsh) used to measure the voltage drop. An inductor linked to the SST was used to compensate the air flux. The energy losses and hysteresis loops for the samples were measured at peak flux densities ranging from 1.0 T to 1.4 T, and magnetizing frequencies ranging from 50 Hz to 800 Hz.

During the measurement, the magnetic field $H(t)$ is generated by the input electrical current $i(t)$ of the primary winding. Meanwhile, the waveform of the secondary induced voltage for sinusoidal excitation is maintained as sinusoidal as possible, achieved using a PID feedback controller [24]. Then, the magnetic flux densities $B(t)$ are derived according to Faraday's law and Lenz's law.

The control loop of the measurement system and field separation is illustrated in Fig. 2. The error between the set point and measured magnetic flux density is calculated by the PID controller, with the input current regulated by controlling the power amplifier. The sinusoidal waveform of magnetic flux density is obtained by maintaining a sinusoidal waveform of the secondary induced voltage. The instantaneous waveforms of the magnetic field and magnetic flux density were obtained for a typical NOES at a magnetizing frequency of 50 Hz and peak flux density of 1.4 T; the results are shown in Fig. 3. from which it is evident that the magnetic flux density lags the magnetic field due to the hysteresis effects.

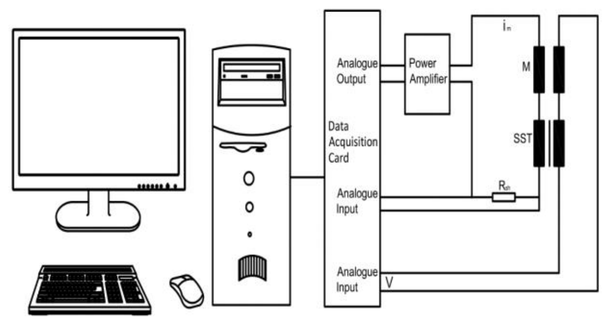

Fig. 1. Schematic diagram of SST measurement system.

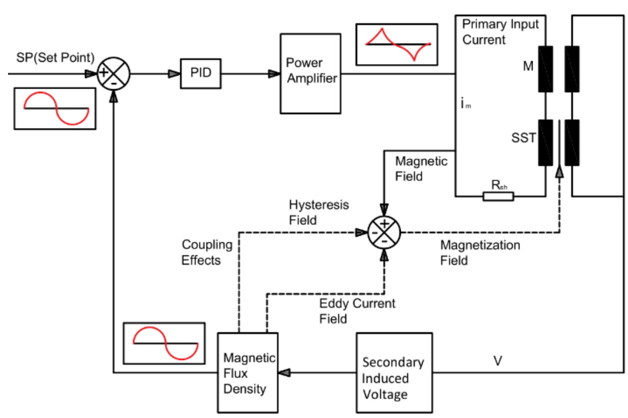

Fig. 2. Control loop and field separation theory

As shown in Fig. 3, the magnetization processes cycle between magnetization and demagnetization. Magnetization occurs in the first and third quadrants of the magnetic flux density, with demagnetization taking place in the second and fourth quadrants. The time rate of change of magnetization is aligned with the magnetization direction ($dB/dt > 0$), while the time rate of change of the demagnetization process is opposite to the magnetization direction ($dB/dt < 0$). So, the output of the PID controller is positive and negative for magnetization and demagnetization, respectively. The WMF [12] of the magnetization coupling effects of individual atomic dipoles is always oriented in the direction of the magnetization. Accordingly, the WMF is positive in the first and second quadrants and negative in the third and fourth quadrants.

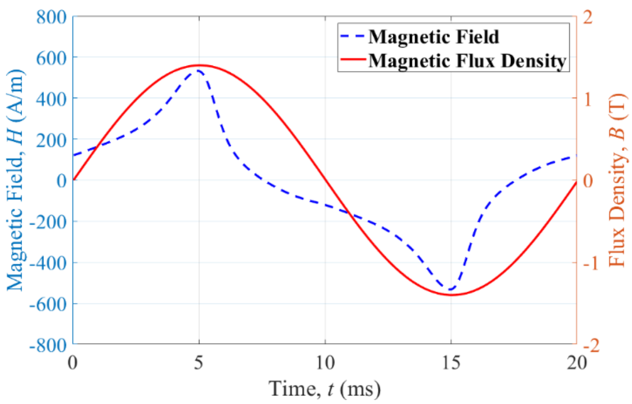

Fig. 3. Instantaneous waveforms of the magnetic field and magnetic flux density at magnetizing frequency of 50 Hz and peak flux density of 1.4 T

The hysteresis field is contributed by the WMF effect described in [11], and the eddy current field generated by the magnetic flux is always opposite to the magnetization direction based on Faraday's law and Lenz's law. As illustrated in Fig. 2, the vector combined field, comprised of the magnetic field, hysteresis field and eddy current field, is the magnetization field driving the magnetization processes.

The time rate of change of the magnetic field is aligned with that of magnetic flux density. So, the WMF and the output of the PID controller are oriented in the same direction in the first and third quadrants of the magnetic flux density and the opposite direction in the second and fourth quadrants. Then, the WMF provides a positive or negative feedback effect during magnetization and demagnetization, respectively. The feedback effects are summarized, according to analysis of the WMF and PID controller output at different quadrants in the magnetic flux density sine waveform for one cycle, in TAB. 1.

Magnetic Flux Density	First quadrant	Second quadrant	Third quadrant	Fourth quadrant
PID output	+	-	-	+
Weiss field	+	+	-	-
Feedback effect	Positive	Negative	Positive	Negative

TAB. 1. Feedback effects based on WMF and PID controller output.

The energy linked to the WMF effect can be described using the Zeeman energy between the WMF and magnetic flux density. The energy generated by the WMF in the first and third quadrants of the magnetic flux density enhances the magnetization processes; the energy linked to the WMF in the second and fourth quadrants has the opposite effect. The WMF feedback effects can be observed in the waveform of the magnetic field shown in Fig. 3, the slope of the magnetic field at the start of the second and fourth quadrants is far larger due to the energy needed to compensate for the WMF negative feedback effects during demagnetization.

In the first and third quadrants, the WMF provides energy to the system to boost the magnetization processes. In contrast, the WMF feeds off the energy from the system to constrain the demagnetization processes. The energy consumed during demagnetization equals the energy produced by WMF during magnetization. So, the WMF positive and negative feedback effects offset each other except at the magnetization tips ($dB/dt = 0$). The WMF reaches a maximum value at the tips when the WMF feedback effect transitions from positive to negative, and this maximum value contributes only to the hysteresis losses if considering the counteraction between the WMF positive and negative feedback effects.

According to Weiss theory [12], the WMF, H_w, can be expressed in terms of the following equation:

$$H_w = \alpha M, \tag{1}$$

where α is the mean field constant and M is the instantaneous magnetization. Then, the WMF feedback energy based on Zeeman energy against the magnetic induction B, W_w, can be expressed as:

$$W_w = \alpha \iint MBdMdB. \tag{2}$$

So, at the saturation tips, all the atomic dipoles in the samples are aligned with the magnetic field direction. All these alignments exert a strong coupling effect on the magnetic field, while this interaction of individual atomic dipoles results in the WMF. Therefore, this study assumed that a magnetic force generated from the coupling effect of the magnetization at the reversal turning point needed to be overcome to continue the reversal demagnetization process. This field is named as hysteresis field H_h, which is the WMF at the magnetization tips, then,

$$H_h \; = \; H_{wp} = \alpha M_p. \tag{3}$$

Where M_p is the magnetization at any order reversal point, and H_{wp} is the WMF created by M_p. According to the definition of coercivity, H_c is the magnetic field required to demagnetize the material. This means the magnetic field at coercivities needs to counteract the WMF at tips so that the magnetic flux density can be reduced to zero. Then, H_h is equal to the coercivity H_c, for magnetic flux density B to be zero. Because the direction of the hysteresis field H_h is opposite to the reversed magnetic field H, the hysteresis field at a positive tip is expressed as:

$$H_h \; = \; H_c, \tag{4}$$

and the hysteresis field at a negative tip as:

$$H_h = -H_c. \tag{5}$$

Then, the astonishing conclusion can be reached that the WMF feedback effects at magnetization tips are the physical origin of the magnetic hysteresis effect.

When the processes change directions from magnetization to demagnetization at the reversal turning point, the excitation source must contribute more energy to compensate for the coupling effect of the magnetization at the tips.

3. A simulation method of magnetic hysteresis

The theme of this paper is the simulation of the magnetization processes of ferromagnetic materials. A simulation method [21] was derived according to the domain patterns in ferromagnetic materials and the excitation field coupling effect. The simulation method is derived based on the assumption that the hysteresis field $H_{\boldsymbol{h}}$ is generated at the reversal turning point when the magnetic field strength H and the magnetic flux density B change their directions. Conventionally, the magnetic field $H(t)$ is produced by the excitation source. In [21], it is assumed that the excitation field $h(t)$ is the vector summation of the magnetic field $H(t)$ and the hysteresis field $H_{\boldsymbol{h}}$, such that:

$$h(t) = H(t) + H_{\boldsymbol{h}}. \tag{6}$$

Then, the excitation field for an ascending curve is obtained as follows:

$$h(t) = H(t) - H_{\boldsymbol{c}}, \tag{7}$$

and the excitation field for descending curve is calculated using the following equation,

$$h(t) = H(t) + H_{\boldsymbol{c}}. \tag{8}$$

Therefore, the excitation field can be easily calculated using experimental data. The curves of $B - h$ are single curves of bijective function without hysteresis effect. It is far easier to explore a single curve than to study a hysteresis loop, which is represented by the one-to-two function with nonlinearity.

GOESs show the best magnetic properties along with the rolling direction because of the grains' orientation, so the properties are dominated by the anisotropic components. NOESs demonstrate identical magnetic properties as per the magnetizing directions because the grains in NOES are randomly oriented other than in just the rolling direction. So, the properties of NOESs are decided by the isotropic components. Nonetheless, there are anisotropic and isotropic structures in both GOESs and NOESs [25-28]. Both anisotropic and isotropic structures determine the magnetic properties in GOES and NOES sheets, so the simulation method of GOES developed in [21] can also be applied to NOES in the same way.

The magnetization processes of the anisotropic structure can be described using the hyperbolic tangent function (9) [21],

$$M_{\boldsymbol{a}} = M_{\boldsymbol{sa}} tanh\left(\frac{\mu_0 m_a h}{kT}\right) = M_{\boldsymbol{sa}} tanh(ah), \tag{9}$$

which was derived based on the variation of the anisotropic domain pattern under an excitation field.

In (9) m_a is the typical unit magnetic moment in the anisotropic domain, and

$$a = \frac{\mu_0 m_a}{kT}, \tag{10}$$

is a coefficient related to the unit moment of the anisotropic magnetic domain and the temperature T. μ_0 is the vacuum permeability, and k is the Boltzmann constant [12]. $M_{\boldsymbol{sa}}$ is the magnetization saturation of the anisotropic component when all the magnetic dipoles in the anisotropic domain are aligned with the excitation field [21].

The isotropic domain moment is randomly oriented in terms of the excitation field. Some moments may coincide with the crystallographic direction; however, most domains have irregular shapes and show a disoriented structure. Driven by the excitation field, the magnetization of the isotropic domain pattern can be expressed as the well-known Langevin function (11), which represents the homogeneous structure in the magnetic material [21]:

$$M_{\boldsymbol{i}} = M_{\boldsymbol{si}}\left(coth(bh) - \frac{1}{bh}\right) = M_{\boldsymbol{si}} L(bh), \tag{11}$$

where,

$$b = \frac{\mu_0 m_i}{kT}, \tag{12}$$

is coefficient related to the unit moment of the isotropic magnetic domain, and the temperature T. m_i is the typical unit magnetic moment in the isotropic domain, while $M_{\boldsymbol{si}}$ is the magnetization saturation of the isotropic components when all the magnetic dipoles in the isotropic domain are aligned with the excitation field [21].

The third component of the simulation method is the coupling effect of the excitation field, which provides a proportion of the magnetic induction B. When the excitation field is excited, the field will generate a part of the magnetic induction and can be expressed as:

$$M_h = \alpha h(t), \tag{13}$$

where α is a coefficient linked to the material microstructure and magnetization conditions. The process of magnetic flux density B versus excitation field h can then be expressed via the following single equation:

$$B = M_a + M_i + M_h, \tag{14}$$

or instead, using the equations (9), (11), and (13), as:

$$B = M_{\boldsymbol{sa}} tanh(ah) + M_{\boldsymbol{si}} L(bh) + \alpha h \tag{15}$$

The magnetization processes of GOESs can be analyzed using the single equation (15), which has proved to deliver an excellent performance [21]. The domain patterns in GOESs and NOESs are identical, although the domain size, grain size and grain orientation in both are different. Therefore, equation (15) is also suitable for describing the magnetization processes of NOESs. Nevertheless, the proportion of anisotropic and isotropic domain structures in GOESs and NOESs varies significantly due to different production procedures, so their magnetic properties show striking divergence. The simulation method is applied to simulate magnetic hysteresis loops and calculate the energy losses of NOESs under controlled sinusoidal excitation.

The simulation method is excellent for generating the sigmoid shape curve. Nonetheless, the measured magnetic hysteresis loops sometimes show irregular and distorted S-shaped curves. To expand (15) to simulate the distorted and irregular curves, the third component is omitted because the coupling effect of the excitation field is far smaller than the other two components in the ferromagnetic material. The hyperbolic tangent and Langevin functions can be replaced by exponential functions, and the magnetic induction expressed via the simplified expression [21]:

$$\boldsymbol{B} = M_{sa}exp(ah) + M_{si}exp(bh). \tag{16}$$

Therefore, when a single curve is deformed and irregularly shaped, the curve can be separated into several sections with one-to-one functions. Equation (16) can be applied to simulate the segment curves. So, equations (15) and (16) are used to simulate the single curves converted from measured hysteresis loops avoiding the need to simulate the hysteresis loops directly.

Conventionally, the magnetic loss is evaluated by calculating the area of the magnetic hysteresis loop. So, the energy loss per cycle in a shin sheet under sinusoidal excitation can be expressed as [29]:

$$W_t = \int BdH, \tag{17}$$

Replacing H with h and considering there are two single curves, the energy loss can be calculated via the following expression:

$$\begin{aligned} W_t &= 2\int Bdh \\ &= 2\int (M_{sa}tanh(ah) + M_{si}L(bh) + \alpha h)dh. \end{aligned} \tag{18}$$

The main advantage of this methodology is that the parameters are related to the microstructure of the magnetic material so that it can also be used to interpret the magnetization processes and analyze energy losses. Meanwhile, the magnetic hysteresis loop can be simulated with high accuracy. The main goal is to prove that the simulation method is a generalised simulation method of magnetization processes for ferromagnetic materials. The analytical simulation method in the form of a single equation is used to describe the magnetic properties and dynamic behavior of NOESs by tracking the hysteresis loops and calculating the energy losses.

4. Simulation Results

The key achievement of the simulations is that the methodology provides a new theory of magnetic hysteresis in the magnetization processes of ferromagnetic materials. This theory based on the WMF at the tips justifies the method to cancel out the hysteresis effect (coercive field) from the measured $B - H$ hysteresis loops to obtain a $B - h$ single curve, which is a curve passing through the origin representing a one-to-one injective function. Then, the simulation of the complicated hysteresis loop can be achieved by tracking the single curve, and the single curve can be used to generate the relevant hysteresis loop. The cancellation of the hysteresis effect is performed using equations (6) and (7).

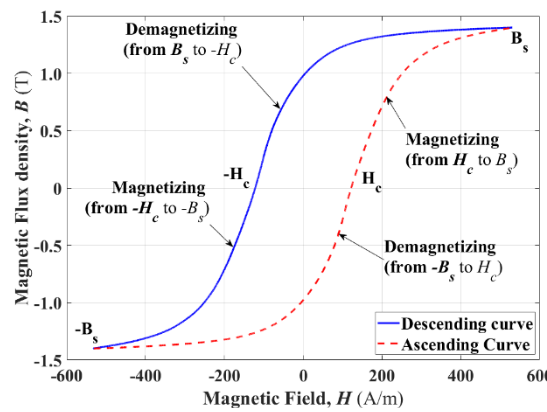

Fig. 4. Hysteresis loop of NOES Measured at 50 Hz and B_{pk} = 1.4 T.

Following the same data processing procedure as in [21], the first step is to consider the controlled sinusoidal magnetic induction of NOESs at a magnetization frequency of 50 Hz and a peak flux density (B_{pk}) of 1.4 T. The same method is used to process the measurements of other frequencies and peak flux densities. As shown in Fig. 4, the measured hysteresis loop includes two s-shape curves, a descending and an ascending one. The descending curve is measured from B_s to $-B_s$. The single curves are separated by coercivities. On the descending curve, the curve segment from B_s to $-H_c$ is a demagnetizing section, and the segment from $-H_c$ to $-B_s$ represents a magnetizing section. The counterpart of the ascending curve is measured from $-B_s$ to B_s segments from $-B_s$ to H_c and H_c to B_s represent demagnetizing and magnetizing curve sections, respectively. The descending and ascending curves constitute a cycle of magnetization.

Equations (7) and (8) are used to offset the hysteresis effect to obtain two single curves without hysteresis. The single curves of B versus h acquired and shown in Fig. 5. After the procedure of cancelling out the hysteresis effect, the descending curve moves to the right a horizontal distance H_c, and the ascending curve shifts to the left ~~at~~ the same distance. The two single curves intersect at the origin. For both descending and ascending curves, the magnetic flux density and excitation field are synchronized. Because of the parallel displacement of the descending and ascending curves to the origin, the two curves are disconnected at the peak flux density tips.

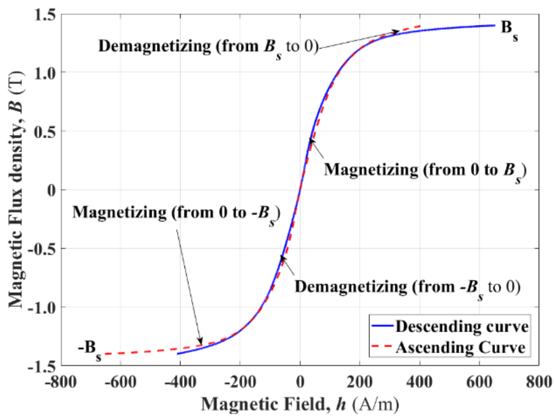

Fig. 5. Single curves of NOES obtained from the hysteresis loop in Fig. 1 by shifting the descending curve to the right at a horizontal distance H_c and ascending curve to the left at the same distance.

It is evident that both single curves in Fig. 5 are smooth s-shaped curves, and the relationship between B and h is a one-to-one function. The injective function of the single curves facilitates the simulation using the single equation (15). In this study, the single curves are investigated first rather than simulating the hysteresis loops directly. The similarity of the two single curves reveals that the magnetic properties of NOES are dominated mainly by isotropic structures leading to similar magnetism regarding the magnetization directions. The gap between the peak flux density tips of two single curves represents the extent of the hysteresis field, which is linked to the magnetization frequencies, peak flux densities, and material microstructures.

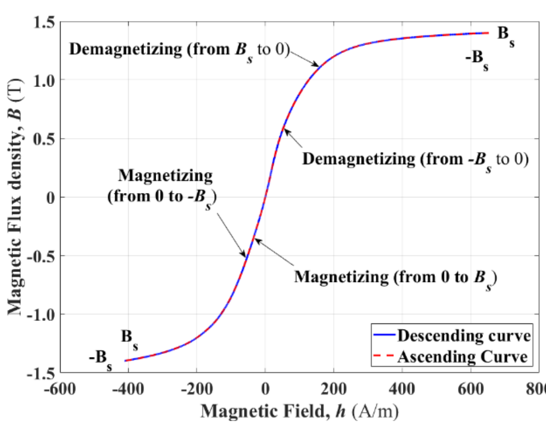

Fig. 6. Two identical single curves of NOES obtained from the curves in Fig. 5 by rotating the ascending curve 180° about the origin.

The magnetization process under a sinusoidal excitation is a cyclic process from magnetization to demagnetization and then magnetization again, and so on. So, the ascending and descending curves are symmetric with respect to the origin. The next step is to manipulate the single curves. The ascending single curve is rotated through 180° about the origin. As shown in Fig. 6, the ascending and descending curves are identical after the rotation. Therefore, the descending curve is chosen to study the magnetic properties instead of tracing the hysteresis loop directly.

The s-shape descending curve of B versus h can be simulated using equation (15). During magnetization and demagnetization, the anisotropic and isotropic domain patterns act in opposite ways correspondingly. So, the magnetization and demagnetization curve sections need to be processed separately to calculate the relevant parameters in equation (15). The measurement data is processed using MATLAB curve fitting tools to conduct a regression analysis [30] using (15); the optimized solver parameters of 50 Hz and 1.4 T can be found in TAB. 2. The simulated single curve created and shown in Fig. 7, and it is identical to the measured descending curve. It is observed that the magnetization is dominated by isotropic structures during the magnetization process, and it is determined by anisotropic components during the demagnetization process.

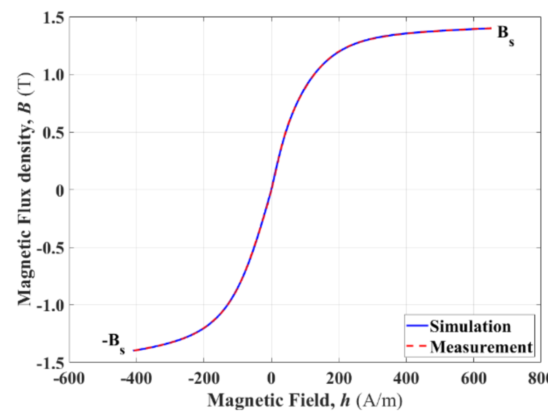

Fig. 7. Comparison of simulated and derived single curves for NOES at 50 Hz and B_{pk} = 1.4 T.

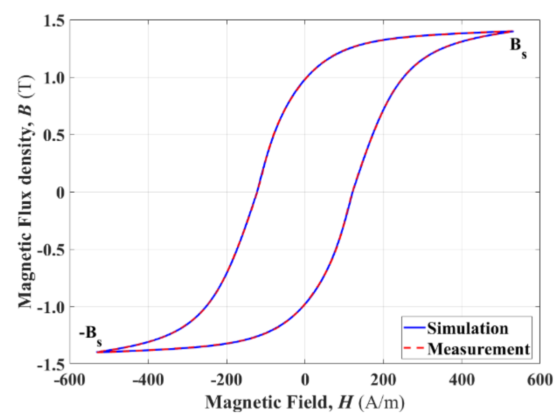

Fig. 8. Comparison of simulated and measured hysteresis loops for NOES at 50 Hz and B_{pk} = 1.4 T.

The simulation method describes the magnetization processes based on the reaction of the microstructures to the external excitation field. Nonetheless, the measured hysteresis loop is described as a function of B versus H. The simulated hysteresis loop is achieved by manipulating the simulated single curve to fit the measured hysteresis loop. The simulated and measured hysteresis loops are shown in Fig. 8, and it is evident that the simulation method performs very well at tracing the magnetic hysteresis loop.

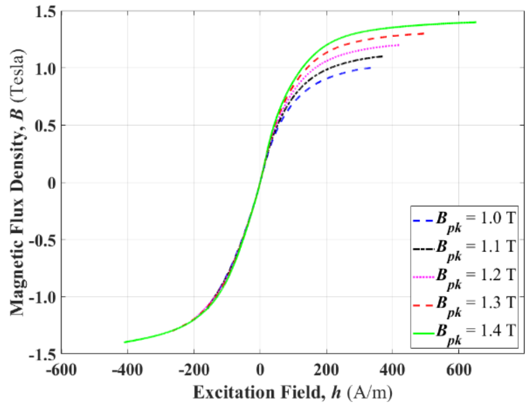

Fig. 9. Single Curves of NOES obtained from the hysteresis loops measured at 50 Hz and B_{pk} from 1.0 to 1.4 T.

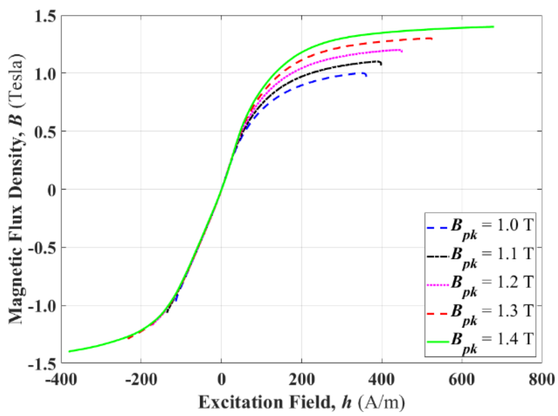

Fig. 10. Single Curves of NOES obtained from the hysteresis loops measured at 100 Hz and B_{pk} from 1.0 to 1.4 T.

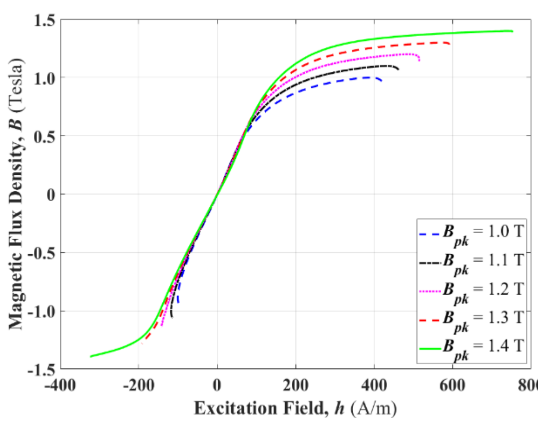

Fig. 11. Single Curves of NOES obtained from the hysteresis loops measured at 200 Hz and B_{pk} from 1.0 to 1.4 T.

The simulation of NOES for a variety of magnetization frequencies and peak flux densities was undertaken using the same method described for the frequency of 50 Hz and peak flux density of 1.4 T. The single curves of B versus h are derived from the measured hysteresis loops for magnetization frequencies from 50 Hz to 800 Hz and peak flux densities from 1.0 T to 1.4 T. The obtained single curves are shown in Figs. 9 to 13, respectively. On these curves, the sections of $h < 0$ represent magnetization, and the sections of $h > 0$ represent demagnetization. The parameters of these two curve sections need to be calculated separately due to the different magnetization mechanisms.

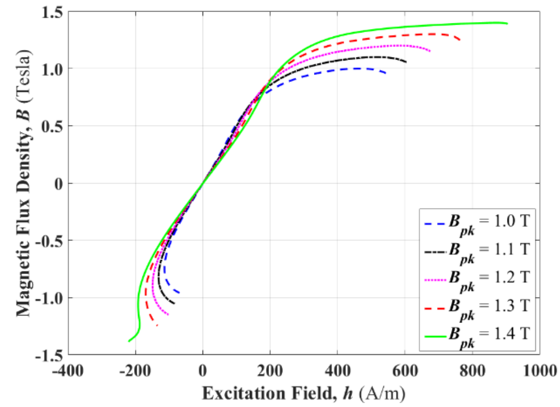

Fig. 12. Single Curves of NOES obtained from the hysteresis loops measured at 400 Hz and B_{pk} from 1.0 to 1.4 T.

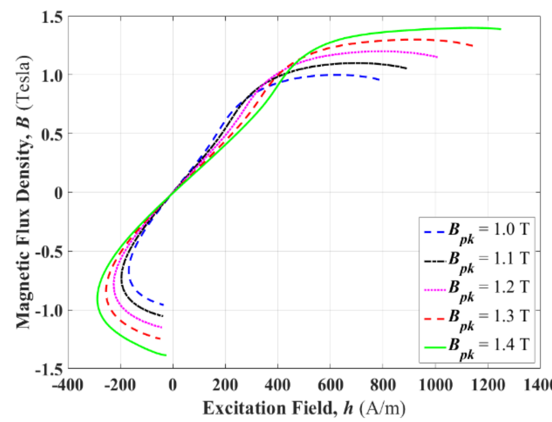

Fig. 13. Single Curves of NOES obtained from the hysteresis loops measured at 800 Hz and B_{pk} from 1.0 to 1.4 T.

One interesting finding from the single curves shown in Fig. 9 to 11 is that these single curves have similar shapes, and all pass the origin. These single curves are the standard s-shape curves that can be simulated using (15). The optimized parameters of (15) magnetized at 50 Hz, and 1.0 T to 1.4 T are listed in TAB. 2. The single curves at 50 Hz and 1.0 T to 1.4 T are simulated by using (15) adopting these parameters. The hysteresis loops at 50 Hz and 1.0 T to 1.4 T are shown in Figs. 15. The parameters shown in TAB. 2 are obtained using regression analysis; however, the isotropic and anisotropic components in ferromagnetic materials are impossible to measure using current measurement technology. Accordingly, the parameters may contain unknowable errors, but it is still possible to distinguish that it is mainly determined by isotropic components during magnetization as the M_{si} is greater the M_{sa}, and it is mainly determined by anisotropic components during demagnetization because the M_{sa} is greater than the M_{si}.

Excitation	Curve section	M_{sa} (T)	M_{si} (T)	a	b	α
50 Hz 1.0 T	Mag.	0.011	0.425	10.95	2.774	0.393
	Demag.	0.468	0.580	1.361	0.961	0.030
50 Hz 1.1 T	Mag.	0.068	1.087	1.090	1.602	0.137
	Demag.	0.663	0.375	0.583	4.333	0.019
50 Hz 1.2 T	Mag.	0.444	0.331	0.922	2.077	0.200
	Demag.	0.726	0.428	0.549	4.051	0.013
50 Hz 1.3 T	Mag.	0.196	1.345	0.456	1.612	0.008
	Demag.	0.768	0.506	0.512	3.691	0.008
50 Hz 1.4 T	Mag.	0.503	0.973	0.722	1.384	0.011
	Demag.	0.846	0.508	0.508	3.658	0.008

TAB. 2. Parameters of equation (15) for creating the magnetizing and demagnetizing curve sections for NOES magnetized at 50 Hz and B_{pk} from 1.0 T to 1.4 T.

Excitation	Curve section	M_{sa} (T)	M_{si} (T)	a	b	α
50 Hz 1.4 T	Mag.	0.503	0.973	0.722	1.384	0.011
	Demag.	0.846	0.508	0.508	3.658	0.008
100 Hz 1.4 T	Mag.	0.840	1.104	0.722	0.451	0.000
	Demag.	0.626	0.875	0.885	1.097	0.000
200 Hz 1.4 T	Mag.	1.323	0.360	0.402	0.678	0.000
	Demag.	0.904	0.564	0.510	0.957	0.000

TAB. 3. Parameters of equation (15) for creating the magnetizing and demagnetizing curve sections for NOES magnetized at frequencies from 50 Hz to 200 Hz and B_{pk} = 1.4 T.

Curve section	M_{sa} (T)	M_{si} (T)	a	b	α
Magnetizing					
Section 1	0.249	-0.242	0.330	-0.352	
Section 2	0.148	0	0.464	9.766	
Section 3	1.642	0	-0.120	7.133	
Section 4	1.567	-0.176	-0.093	-0.859	
Demagnetizing					
Section 1	-0.800	1.4	-9.01	0.239	-0.028
Section 2	3.408	0.694	-2.406	0.694	-0.110
Section 3	14.91	-24.57	0.352	0.739	0.961

TAB. 4. Parameters associated with equation (15) for magnetizing sections and (16) for demagnetizing sections used to obtain the contiguous magnetizing and demagnetizing curve sections of Fig. 14 for NOES magnetized at 800 Hz and 1.4 T.

TAB. 3 shows the optimized parameters of (15) magnetized at frequencies from 50 Hz to 200 Hz and peak flux density of 1.4 T. The relevant single curves are simulated using (15) adopting these parameters, and the corresponding hysteresis loops are plotted using the same method shown in Figs. 8. Physically, the sum of M_{sa} and M_{si} should be around the peak flux density because the third component of (15) is very small. So, the parameters of magnetization at 50 Hz and 1.0 T loose their physical meaning. Theoretically, the proportionality of M_{sa} and M_{si} is mainly determined by the materials and the magnetization directions and is less linked to the magnetization frequencies and peak flux densities. The dependency of the magnetic losses regarding the magnetization frequencies and peak flux densities will be explored in future work.

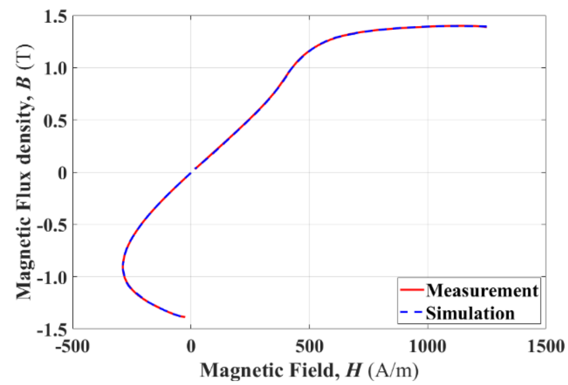

Fig. 14. Simulated contiguous curve sections, 4 in total for magnetizing section using (16), 3 in total for demagnetizing section using (15), superimposed on the corresponding measured single curve for NOES at 800 Hz and B_{pk} = 1.4 T.

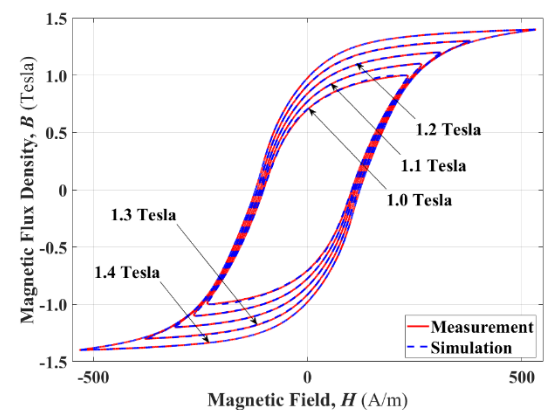

Fig. 15. Comparison between simulated and measured hysteresis loops for NOES at 50 Hz and B_{pk} from 1.0 T to 1.4 T.

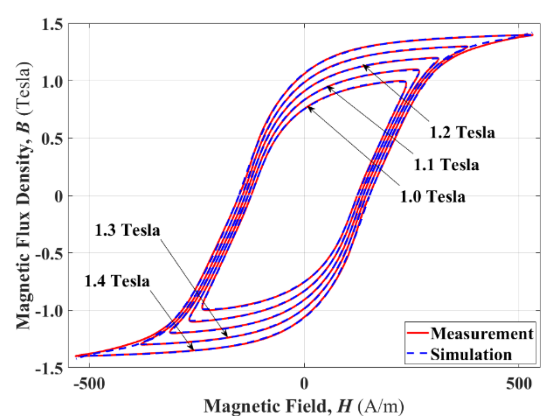

Fig. 16. Comparison between simulated and measured hysteresis loops for NOES at 100 Hz and B_{pk} from 1.0 T to 1.4 T.

As shown in Fig. 12 and 13, the single curves at 400 Hz and 800 Hz reveal curl at magnetization section tips, which reveals the asynchronous phenomena introduced by high frequencies. When the excitation fields reach maximum values and start to reverse their directions, the flux densities are still increasing. It gives a sense that the flux densities go ahead of the excitation field. These asynchronous phenomena caused by high frequencies make the calculation of parameters rather intricate, so the simulation of the single curves must be performed by fitting the piecewise curves using (15) or (16). The parameters used in (15) or (16) must be calculated for each segment separately; the more segments used, the higher the accuracy of the simulation. The calculation of the segmented parameters is conducted separately for the magnetization and demagnetization sections.

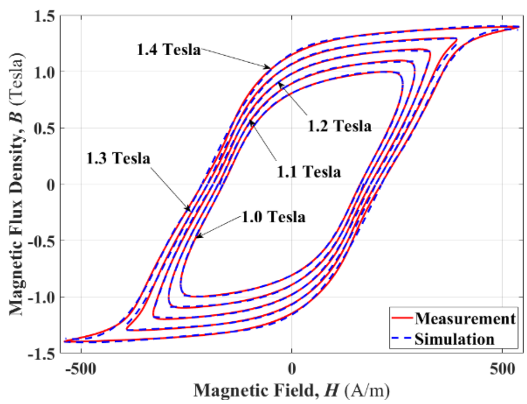

Fig. 17. Comparison between simulated and measured hysteresis loops for NOES at 200 Hz and B_{pk} from 1.0 T to 1.4 T.

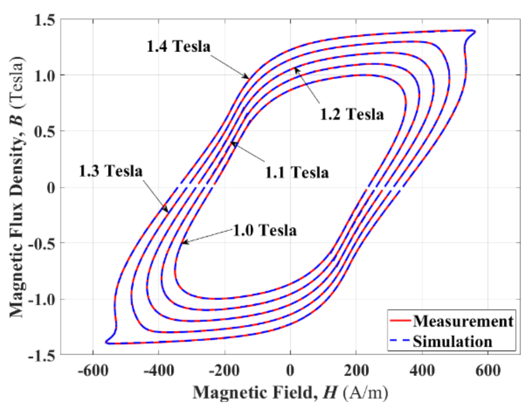

Fig. 18. Comparison between simulated and measured hysteresis loops for NOES at 400 Hz and B_{pk} from 1.0 T to 1.4 T.

For the cases of 800 Hz and 1.4 T, the simulation of the $B-h$ curve is conducted in a piecewise fashion. The magnetizing section is separated into four segments and simulated using (16), whereas the demagnetizing section is divided into three segments and simulated using (15). The parameters calculated are listed in TAB. 4. The parameters obtained using the MATLAB fitting tool in the piecewise method cannot represent the authentic physical meaning of the magnetization processes. The simulated single curve is shown in Figs. 14. It is evident from the figure that equations (15) and (16) can reproduce the single curve with remarkable similarity. Then, the hysteresis loops of the test sample can be created using the simulation method for the range of magnetization.

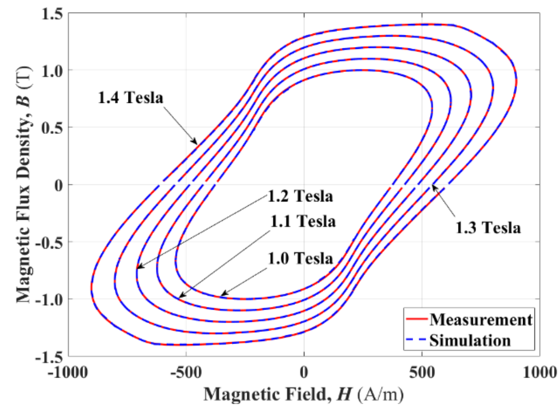

Fig. 19. Comparison between simulated and measured hysteresis loops for NOES at 800 Hz and B_{pk} from 1.0 T to 1.4 T.

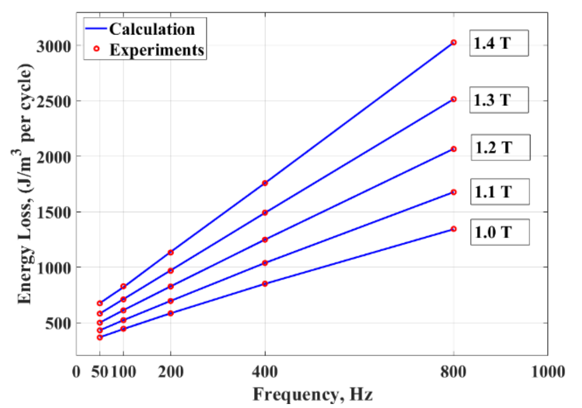

Fig. 20. Comparison between calculated and measured energy losses for NOESs magnetized at frequencies ranging from 50 to 800 Hz and B_{pk} from 1.0 to 1.4 T.

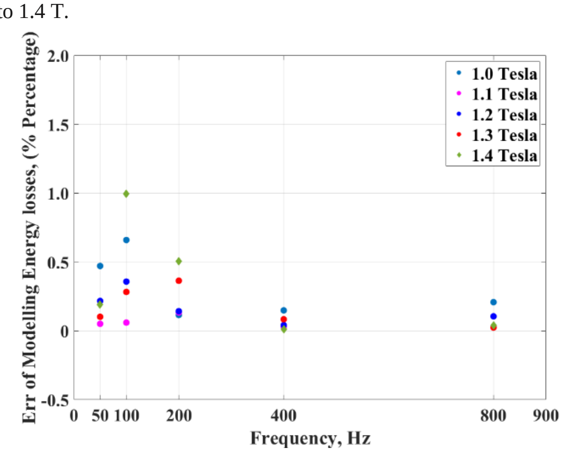

Fig. 21. Errors for NOESs between calculated and measured energy losses at frequencies ranging from 50 to 800 Hz and B_{pk} from 1.0 T to 1.4 T.

The measured and calculated hysteresis loops at magnetization frequencies of 50 Hz to 800 Hz and peak flux densities of 1.0 T to 1.4 T are illustrated in Fig. 15 to 19, respectively. The results indicate that the calculated loops are consistent with the measured hysteresis loops in the range of measurement frequency and magnetic flux density. Evidently, the simulation method according to the domain theory can reproduce the magnetic hysteresis loops of NOESs with remarkable accuracy. This simulation method is also convenient for evaluating the energy loss using equation (18), which is used to calculate the

Zeeman energy between the excitation field and magnetic flux density.

Fig. 20 compares the calculated and measured energy losses at the magnetization frequencies from 50 Hz to 800 Hz and the peak flux densities from 1.0 T to 1.4 T. Fig. 21 demonstrates the errors between the calculated and measured energy losses. It is observed that the maximum difference with the measurement data is less than 1% in close agreement.

5. Conclusions and Future Work

In this study, a simulation method having a sound physical underpinning is used to reproduce the magnetic hysteresis loops of NOESs with isotropic characteristics. This single equation simulation has already been verified for GOESs with strong anisotropic characteristics [21]. Accordingly, the simulation method is applicable to both homogeneous and inhomogeneous materials. Meanwhile, the energy loss per cycle can be calculated by simply integrating the single equation over the range of the excitation field. The energy losses are calculated for NOESs over a wide range of magnetization frequencies and flux densities. The results obtained show that this method performs very well for tracing the major and minor loops of NOESs. It is also the first-time energy loss has been calculated using a single equation with such a high level of accuracy.

The results of this study demonstrate the reliability of the simulation methodology in predicting the magnetic hysteresis behavior of NOESs for a range of magnetization. Despite the single equation being currently the simplest simulation method of magnetic hysteresis, it has a sound physical underpinning and fills a technology gap for interpreting the magnetization processes of ferromagnetic materials. Compared to previous simulation methods, the one described here is simple to implement and needs far fewer calculations.

In addition to showing a critical step forward in interpreting the magnetization process related to soft magnetic materials under sinusoidal excitation, the proposed simulation method is also capable of investigating magnetic behavior under non-sinusoidal excitation widely applied in renewable energy systems, which is currently under investigation. The insights might be of interest to the physicists and engineers that endeavour to improve the performance of magnetic components in power electronics.

Acknowledgement

The authors are grateful to Cogent Power Ltd. for providing the electrical steel sheets, and Cardiff University for the experimental results.

References

[1] P. Beckley, "Electrical Steels: A Handbook for Producers and Users," First edition, European Electrical Steels, Newport, South Wales, 2000.
[2] S. Zhang, B. Ducharne, S. Takeda, G. Sebald and T. Uchimoto, J. Magn. Magn. Mater., 538, p.168278, 2021.
[3] M. Noori and W.A. Altabey, Appl. Scie., 12(19), p.9428, 2022.
[4] J.A. Ewing, Magnetic induction in iron and other metals. D. Van Nostrand Company, 1900.
[5] C. Arimatea and D. Jacquet, Mesure de l'influence magnétique du cycle proton 450 GeV sur le cycle positron (No. SL-Note-2001-013-MD). CERN-SL-Note-2001-013-MD, 2001.
[6] M. Kersten, Zur Deutung der Koerzitivkraft. In Probleme der Technischen Magnetisierungskurve (pp. 42-72). Springer, Berlin, Heidelberg, 1938.
[7] M. Kersten, "Grundlagen einer Theorie der ferromagnetischen Hysterese und der Koerzitivkraft." JW Edwards, 1946.
[8] R. Becker and W. Doring, Ferromagnetizmus (Springer, Berlin, 1939).
[9] S. Takahashi and S. Kobayashi, IEEE Trans. on Magn., 44(11), pp.3859-3862, 2008.
[10] F. Henrotte and K. Hameyer, IEEE Trans. on Magn., 42(4), pp. 899-902, 2006.
[11] R.G. Harrison, IEEE trans. on Magn., 45(4), pp.1922-1939, 2009.
[12] D. C. Jiles, Introduction to Magnetizm and Magnetic Materials (Chapman & Hall, London, 1998).
[13] D. C. Jiles and D. L. Atherton, J. Appl. Phys. 55(6), pp. 2115, 1984.
[14] S. Zhang, B. Ducharne, S. Takeda, G. Sebald and T. Uchimoto, J. Magn. Magn. Mater., 531, p.167971, 2021.
[15] A. Ramesh, D. Jiles, and J. Roderick, IEEE Trans. on Magn., 32(5), pp.4234, 1996.
[16] R. Szewczyk, Materials, 7(7), pp.5109, 2014.
[17] I. D. Mayergoyz, Mathematical models of hysteresis and their applications. New York NY: Academic Press, 2003.
[18] R. Zeinali, D. Krop and E. Lomonova, IEEE Trans. on Magn., 57(6), pp.1-4, 2021.
[19] S. Bobbio, G. Milano, C. Serpico, and C. Visone, IEEE Trans. on Magn., 33(6), pp. 4417, 1997.
[20] Y. Li, J. Zhu, Y. Li and L. Zhu, J. Magn. Magn. Mater., 544, p.168655, 2022.
[21] Z. Zhang, H, Hamzehbahmani, and P. H. Gaskell, IEEE Trans. on Magn., 58(1), pp.1-9, 2021.
[22] BS EN 10280:2001 + A1:2007, Magnetic Materials - Methods of measurement of the magnetic properties of electrical sheet and strip by means of a single sheet tester, British Standard.
[23] H. Hamzehbahmani, Development of novel techniques for the assessment of inter-laminar resistance in transformer and reactor cores (Doctoral dissertation, Cardiff University), 2014.
[24] O. de la Barrière, C. Appino, C. Ragusa, F. Fiorillo, M. LoBue and F. Mazaleyrat, IEEE Trans. on Magn., 54(9), pp.1-15, 2018.
[25] M. Birsan, and J.A. Szpunar, J. Appl. Phys., 81(2), pp.821-823, 1997.
[26] H. Pirgazi, R.H. Petrov and L.A. Kestens, Steel Research Rnternational, 87(2), pp.210-218, 2016.
[27] G.H. Shirkoohi and M.A.M. Arikat, IEEE Trans. on Magn., 30(2), pp.928-930, 1994.
[28] G.H. Shirkoohi and J. Liu, IEEE Trans. on Magn., 30(2), pp.1078-1080, 1994.
[29] F. Fiorillo, C. Appino, M. Pasquale, and G. Bertotti, Hysteresis in magnetic materials. The Science of Hysteresis, vol. 3, pp.1-190, 2006.
[30] The MathWorks, I., 2020. Curve Fitting Toolbox, Natick, Massachusetts, United State. Available at: https://www.mathworks.com/products/curvefitting.html.